

# Introducing BigMag – A Novel System for 3D Magnetic Actuation of Flexible Surgical Manipulators

Jakub Sikorski, Imro Dawson, Alper Denasi, Edsko E.G. Hekman and Sarthak Misra

**Abstract**— Magnetic interaction can be utilized for remote actuation of surgical manipulators. However, platforms currently available for that purpose have limited workspaces, inadequate field strength or very low bandwidth of the electrical subsystem. In this paper, we present BigMag, a novel platform capable of magnetic steering of continuum manipulators for medical purposes. BigMag comprises of 6 mobile coils and is capable of generating the fields of at least 40 mT in any direction at every point of its workspace. Moreover, we introduce a mathematical model for 3D mobile coil arrays. Each coil is modelled using finite element data adjusted by measurement-based correction, (a maximum observed mean error between the model and the prediction of  $3.36 \pm 5.62\%$ ). The model for a full system is validated in two tasks. In the first task, the system executes a prescribed rotating field (mean error between the model and measurement of 7.51% and minimum  $R^2$  of 0.964). The second task tests the estimation of the field for known 3D trajectories (minimum  $R^2$  of 0.967). The investigation concludes with a demonstration of BigMag capabilities in actuation of magnetic catheters in confined spaces using user-controlled steering.

## I. INTRODUCTION

Robotic systems have the potential to revolutionize minimally invasive surgical procedures [1]. One group of devices particularly explored for applications within that field are continuum manipulators [2]. They differ from classical rigid-link manipulators by having a hyper-redundant structure of continuously bending, elastic elements [3]. They are well-suited for medical procedures, due to their inherent compliance. This property allows them for safe operation in confined cavities of human body, even if unwanted contact with tissue was to occur [4]. In particular, numerous attempts have been made to use continuum manipulators to create robotic endovascular catheters [5].

The challenge of developing reliable remote actuation for continuum manipulators has been addressed in multiple works. The most conventional approach involves displacing tendons [6], [7], or elastic tubes [8]. However, the moving parts experience significant friction, making the steering imprecise and subjected to hysteresis, and calling for an alternative [9].

Since the introduction of low-frequency magnetic steering of surgical devices the subject has gained significant attention [10]. The strength and reliability of magnetic interaction are

The authors are affiliated with Surgical Robotics Laboratory (Department of Biomechanical Engineering), and MIRA - Institute for Biomedical Technology and Technical Medicine, University of Twente, 7500 AE Enschede, The Netherlands. S. Misra is also affiliated with the Department of Biomedical Engineering, University of Groningen and University Medical Centre Groningen, 9713 GZ Groningen, The Netherlands.

This research has received funding from the European Research Council (ERC) under the European Unions Horizon 2020 Research and Innovation programme (Grant Agreement #638428 - project ROBOTAR).

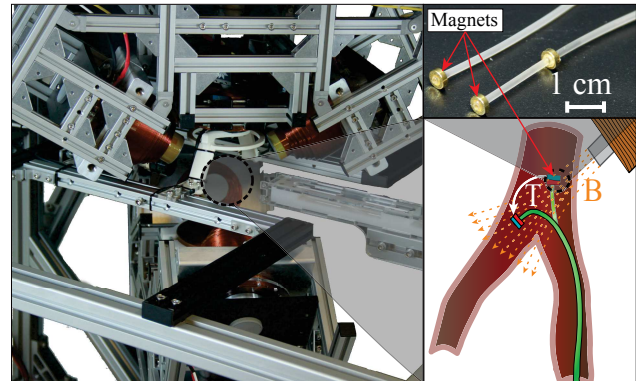


Fig. 1. Automation of flexible surgical manipulators requires reliable actuation. Such actuation is possible by equipping the manipulators with permanent magnets, which interact with external magnetic field ( $B$ ). Torque ( $T$ ), produced as a result of this interaction, deflects the manipulator. This paper presents BigMag - a device using an array of mobile coils to generate arbitrary magnetic fields inside clinically-relevant spaces. Those fields are strong enough to achieve 3D steering of continuum manipulators. Left: functional workspace of BigMag - a sphere with a diameter of 10 cm. Right top: examples of relevant manipulators, equipped with magnets. Right bottom: a target clinical scenario - steering of a flexible manipulator inside the vasculature.

sufficient for actuation of continuum manipulators inserted into human body. Moreover, magnetic fields pose no radiation hazard and thus they may be used even for lengthy surgical procedures. [11].

Several small-scale custom devices for magnetic actuation of continuum manipulators have been presented in the literature [12], [13]. However, the limited operational workspace of those designs narrows their clinical relevance. Increasing the workspace is a challenging task subjected to scalability problems. Enlarging the static coils used in those devices increases their inductance, which limits the bandwidth of the effective magnetic field control. Therefore, this actuation method is inadequate for tasks requiring high control frequency, such as compensation for tissue motion, or force control. Recently, the problem of limited actuation bandwidth of static coil arrays has been reported within a device with enlarged bore [14].

The Niobe<sup>®</sup> system (Stereotaxis Inc., St. Louis, USA) employs permanent magnets instead of coils to address the problem of achieving strong magnetic fields in a large workspace [15]. However, the steering of magnetic field generated by permanent magnets is a challenging task. In Niobe<sup>®</sup> it is achieved by controlling the pose of the magnets. Due to large inertias and a limited range of motion of the permanent magnets, this solution does not present any substantial advantage regarding the bandwidth of the system. Moreover, this method of generating magnetic fields raises safety concerns, as the fields of the magnets cannot be switched off.

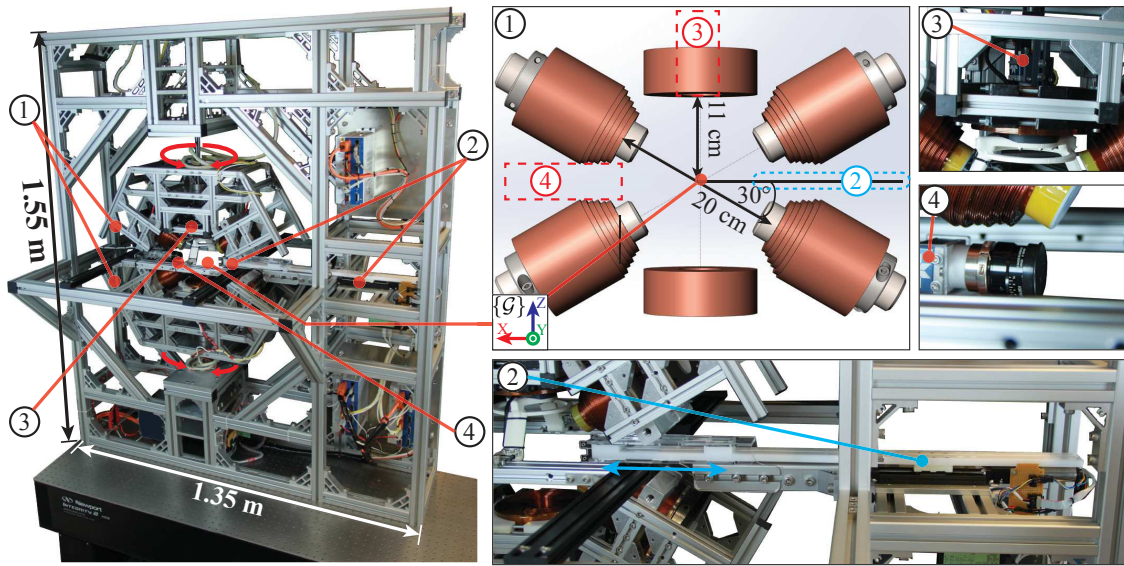


Fig. 2. BigMag consists of an array of six coils mounted on two symmetric mobile frames. Each frame hosts 3 coils. Left: The overview of the system. Right: key elements of the system. ① Mobile Coils ② Automated inserter of continuum manipulators ③ Top camera ④ Side camera.

In our preceding work, we demonstrated that a magnetic catheter can be steered in 2D using an array of stationary Helmholtz coils under ultrasound guidance [16]. In this article we introduce and characterize BigMag. It is a proof-of-concept system using six mobile coils for 3D magnetic actuation of continuum manipulators (Figure 1). We also propose and validate a model of the magnetic field inside the functional workspace of BigMag. Such a model is required to apply known magnetic wrenches to continuum manipulators. In contrast to most existing devices, the coils of BigMag rotate around its workspace. Numerous advantages of such an approach have been already discussed in the literature [17]. The small size of the mobile coils of BigMag limits both their inertia and inductance, increasing the total bandwidth of the system. To the authors' best knowledge, BigMag is the first device using mobile coils for 3D steering of continuum manipulators.

The rest of the paper is structured as follows: Section II introduces BigMag and explains its design rationale. Section III presents a mathematical model for the magnetic fields, which is used to describe BigMag. Subsequent validation of the model is presented in Section IV, along with a demonstration of BigMag being used in manual steering of magnetic catheters. The paper is concluded by Section V presenting the directions for future work.

## II. DESIGN OF BIGMAG

BigMag has been designed through an iterative process in an attempt to optimize most of its parameters. The goal of the investigation is to meet the field requirements for the selected workspace. This section describes the rationale behind that process. It also presents the architecture of the BigMag with all its subsystems, and key parameters (see Figure 2).

### A. Design Rationale

In order to establish the requirements for the system, let us consider a continuum manipulator with magnets attached to its body. The strength of a magnet located at position ( $\mathbf{p} \in \mathbb{R}^3$ ) is defined by its magnetic dipole moment

TABLE I  
DESIGN REQUIREMENTS FOR BIGMAG

Requirement	Motivation
Spherical effective workspace with a diameter of 10 cm	This volume corresponds to human heart. It considered sufficient for <i>ex vivo</i> trials on biological tissue. [20]
Generation of fields of at least 40 mT in arbitrary 3D direction at any point inside the workspace.	Based on previous research, fields of 40 mT were considered sufficient for effective actuation of surgical continuum manipulators [16].
Magnetic actuation of microrobotic agents.	Such capability increases the range of possible applications of the system.
Automated insertion of continuum manipulators inside the workspace	This allows for simulation of clinically-relevant steering tasks.

( $\mathbf{m} \in \mathbb{R}^3$ ). This dipole interact with the external magnetic field ( $\mathbf{B}(\mathbf{p}) \in \mathbb{R}^3$ ), experiencing a wrench ( $\mathbf{W} \in \mathbb{R}^6$ ), comprising of force ( $\mathbf{F} \in \mathbb{R}^3$ ) and torque ( $\mathbf{T} \in \mathbb{R}^3$ )

$$\mathbf{W} = \begin{bmatrix} \mathbf{F} \\ \mathbf{T} \end{bmatrix} = \begin{bmatrix} \nabla(\mathbf{m} \cdot \mathbf{B}(\mathbf{p})) \\ \mathbf{m} \times \mathbf{B}(\mathbf{p}) \end{bmatrix}. \quad (1)$$

The generation of spatial gradients ( $\nabla \mathbf{B} \in \mathbb{R}^{3 \times 3}$ ) to steer a continuum manipulator was reported infeasible, even for smaller workspaces [18], [19]. It is challenging to achieve forces of adequate magnitudes. Therefore, the application of torque ( $\mathbf{T}$ ) has been selected as the primary actuation method of continuum manipulators. Following that decision, the design requirements for the system have been established, and are presented in Table I.

BigMag is the realisation of the system following these criteria. It comprises of six coils (Table II), held in two symmetrical frames. Three coils are suspended above the horizontal centre plane of the workspace, the other three are located below it. Such an arrangement is proposed in order to make the workspace accessible through its centre plane with 360° clearance.

### B. BigMag - General Overview

The two mobile frames of BigMag are actuated by Maxon EC60 series BLDC motors (Maxon Motors, Sachseln,

Switzerland). They rotate independently along a common, vertical axis at speeds up to 30 RPM. The motors are controlled by iPOS4808 BX-CAT (Technosoft Motion, Neuchâtel, Switzerland) motion controllers. The current in each coil (up to a maximum of 8 A) is controlled using Copley XE-230-20 amplifiers (Copley Controls, Canton, USA)

BigMag hosts 2 Dalsa Genie Nano-C1940 (Waterloo, Ontario, Canada) cameras, allowing for visualization of the entire workspace. Moreover, the system is equipped with an automated advancer. It allows for insertion of continuum manipulators with diameters between 1 and 5 mm. The advancer is steered by a linear actuation unit, comprising of a LX20 linear stage (Misumi Europa GmbH, Schwalbach am Taunus, Germany) powered by a Maxon EC22 motor, and controlled by an iPOS4808 BX-CAT motion controller.

Stepped coils of BigMag are equipped with soft iron cores (Sekels GmbH, Ober-Moerlen, Germany) to increase the field strength. The ring-shaped coils do not contain iron cores. This allows for generation of magnetic fields along the vertical axis with higher bandwidth (200 Hz). In total, BigMag is capable of generating 40 mT in any arbitrary direction (maximum 70 mT in the centre of the workspace) at every point within its workspace. The field of each coil of BigMag can be controlled independently. Exploiting this property, highly non-homogeneous fields can be shaped. The gradients ( $\|\nabla\mathbf{B}\|_2$ ) of magnetic fields of up to 1 T/m were measured inside the workspace. Such gradients are insufficient for actuation of continuum manipulators, but can be used in steering of microrobotic agents using BigMag.

### III. MODELLING OF BIGMAG COIL ARRAY

In order to effectively steer a continuum manipulator, the magnetic field should be known at any location within the workspace. This task is challenging, since the magnetic field of BigMag is non-homogeneous. Moreover, the actual field ( $\mathbf{B}(\mathbf{p})$ ) varies depending on the positions of mobile coils. Therefore, it is essential to develop an accurate model of the field distribution for every state of the system.

#### A. Mathematical Model of a Single Coil

The investigation starts of with a field model, for a single solenoid ( $k \in \mathbb{N}$ ) of fixed dimensions and material composition. The magnetic field generated by such device at point ( $\mathbf{p}$ ) depends on its position in relation to the coil and the current ( $I \in \mathbb{R}$ ) running through the coil. A local frame of reference  $\{\mathcal{C}_k\}$  is constructed for every coil to describe this relationship. The position of  $\mathbf{p}$  expressed in frame  $\{\mathcal{C}_k\}$  is as follows:

$$\mathbf{p}_{\mathcal{C}_k} = \begin{bmatrix} x^{\mathcal{C}_k} & y^{\mathcal{C}_k} & z^{\mathcal{C}_k} \end{bmatrix}^T. \quad (2)$$

Therefore, the magnetic field vector at  $\mathbf{p}_{\mathcal{C}_k}$  is given by

$$\mathbf{B}_{\mathcal{C}_k} = \begin{bmatrix} B_x^{\mathcal{C}_k} & B_y^{\mathcal{C}_k} & B_z^{\mathcal{C}_k} \end{bmatrix}^T. \quad (3)$$

We assume that the saturation of the core material of coil ( $k$ ) is never reached. Thus, the field generated by the actuator can be approximated as linearly dependent on the current ( $I_k \in \mathbb{R}$ ) [12], [21]. Hence, we can simplify the modelling

TABLE II  
SPECIFICATION OF BIGMAG ELECTROMAGNETIC COILS

Specification	Iron-Cored Coil	Air-Cored Coil
Inner Diameter [mm]	45	50
Outer Diameter [mm]	Stepped: (Maximum) 102 (Minimum) 56.3	130
Height [mm]	120	50
Core Length [mm]	180	-
Number of Turns	1596	1021
Resistance [ $\Omega$ ]	4.2	3.4
Cut-off Frequency (Approximately) [Hz]	40	200

by calculating the  $\mathbf{B}_{\mathcal{C}_k}$  for  $I_u$  defined as unit current. The field distribution ( $\widehat{\mathbf{B}}_{\mathcal{C}_k}$ ) obtained this way scales linearly with the current ( $I_k$ ) as follows:

$$\mathbf{B}_{\mathcal{C}_k} = I_k \widehat{\mathbf{B}}_{\mathcal{C}_k}. \quad (4)$$

There are multiple ways of modelling the field distribution ( $\widehat{\mathbf{B}}_{\mathcal{C}_k}$ ), either numerically, or by fitting an analytical function [12], [13], [22]. The choice of a particular method has no influence on the framework.

#### B. Mathematical Model of the Array of Mobile Coils

Assuming the principle of superposition [23] we use the model presented above to represent each coil of BigMag. We define a global reference frame  $\{\mathcal{G}\}$  located in the centre of the workspace (see Figures 2 and 3), such that  $\mathbf{R}_{\mathcal{C}_k}^{\mathcal{G}} \in SO(3)$ , describes the orientation of frame  $\{\mathcal{C}_k\}$  for every coil ( $k \in [1, n]$ ).

An arbitrary point ( $\mathbf{p} \in \mathbb{R}^3$ ) is defined within the workspace. Its position in frame  $\{\mathcal{G}\}$  is described by  $\mathbf{p}_{\mathcal{G}} \in \mathbb{R}^3$  – analogously to (2). Hence, the field ( $\mathbf{B}_{\mathcal{G}}^k$ ) generated by the coil ( $k$ ), is represented as  $\mathbf{B}_{\mathcal{G}}^k = \mathbf{R}_{\mathcal{C}_k}^{\mathcal{G}} \mathbf{B}_{\mathcal{C}_k}^k$ . For every coil, the distance ( $r_k$ ) from global frame  $\{\mathcal{G}\}$  to its local frame  $\{\mathcal{C}_k\}$  is constant. Hence, we can simplify the coordinate transformation between the two frames. By orienting the  $X$  axis of frame  $\{\mathcal{C}_k\}$ , such that it points towards the origin of frame  $\{\mathcal{G}\}$ , we develop the following relation:

$$\mathbf{p}_{\mathcal{C}_k} = \mathbf{R}_{\mathcal{C}_k}^{\mathcal{G}} \mathbf{p}_{\mathcal{G}} + \begin{bmatrix} r_k & 0 & 0 \end{bmatrix}^T. \quad (5)$$

Hence, using (3), (4) and (5), the total field ( $\mathbf{B}_{\mathcal{G}} \in \mathbb{R}^3$ ) of the system is modelled as follows:

$$\mathbf{B}_{\mathcal{G}} = \sum_{i=1}^n I_i \mathbf{R}_{\mathcal{C}_i}^{\mathcal{G}} \widehat{\mathbf{B}}_{\mathcal{C}_i}^i \in \mathbb{R}^3. \quad (6)$$

This model in conjunction with (1) is used to map currents and positions of the coils to wrenches experienced by the manipulator inside the workspace of BigMag.

### IV. VALIDATION OF FIELD MODEL FOR BIGMAG

This section presents three investigations used to test the performance of BigMag and the mathematical models associated with it. First, the representation of the field for a single coil is developed by calibrating a solution of finite element simulation using experimental data. The results of that procedure are then used to validate the model presented in Section III. Final experiment is conducted to demonstrate the capability of BigMag to actuate continuum manipulator using manual steering.

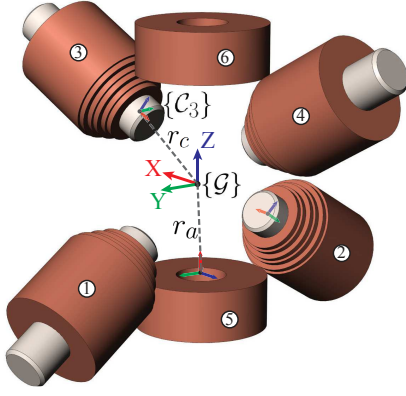


Fig. 3. The overview of the proposed kinematic framework. The global reference frame  $\{G\}$  is located in the centre of the workspace. Local frames  $\{C_k\}, k \in \mathbb{N}, k \in [1, 6]$ , are placed on the long axis of the coils, on their faces oriented towards the workspace, such that their  $X$  axes point towards the origin of frame  $\{G\}$ . Variables ( $r_c$  and  $r_a$ ) denote constant distances to BigMag coils. For  $k \in [1, 4], r_k = r_c = 100$  mm, and for  $k \in [5, 6], r_k = r_a = 110$  mm.

#### A. Device-specific Coil Model

The modelling approach used for BigMag requires the relation (4) to be established for both types of coils. We use a trilinear interpolation of a finite element field model (COMSOL Multiphysics 5.2, COMSOL Inc., Burlington, USA) for that purpose. This method allows to estimate fields at any location ( $\mathbf{p}_{C_k}$ ). Such models, however are prone to errors. Therefore we perform a calibration routine based on measurements to alleviate this.

The magnetic field generated by each type of coil is sampled at a selection of known locations (Figure 4). The collected data are used to calibrate the model of the field, using least squares method. Previous works proposed constant coefficient ( $\alpha$ ) to adjust the field estimated by a model of the coil, such that  $\|\hat{\mathbf{B}}_a(\mathbf{p}_{C_k})\| = \alpha \|\hat{\mathbf{B}}_m(\mathbf{p}_{C_k})\|$ , where ( $\hat{\mathbf{B}}_a \in \mathbb{R}^3$ ) is the calibrated field, ( $\hat{\mathbf{B}}_m \in \mathbb{R}^3$ ) is the estimate from the model and  $\alpha \in \mathbb{R}$  is the linear coefficient [12]. This approach however is insufficient for the large workspace of BigMag. We have observed empirically that the model error depends on the distance of the point ( $\mathbf{p}_{C_k}$ ) from the coil. Therefore, we use the following calibration equation:

$$\|\hat{\mathbf{B}}_a(\mathbf{p}_{C_k})\| = (\alpha + \gamma \|\mathbf{p}_{C_k}\|^\epsilon) \|\hat{\mathbf{B}}_m(\mathbf{p}_{C_k})\|, \quad (7)$$

where  $\alpha, \gamma \in \mathbb{R}$  are constants and where  $\epsilon \in \mathbb{N}$  is an arbitrary exponent.

An experiment (see Figure 4) is performed to validate the proposed calibration routine. It involves dividing the measurements into two datasets. Data measured at the calibration region are used to solve (7) for  $\alpha$  and  $\gamma$  at different values of  $\epsilon$ . The calibrated model is then used to generate the estimates of the field for the points in validation region. The validity of the calibration is tested by comparing estimated values for the validation region against the respective measurements. The results are presented in Table III and Figure 5. They show that our routine is more effective (mean error of 3.36%) than the approach already proposed in the literature (mean error of 8.35%) [12]. The errors for field orientation are below  $0.1^\circ$  in all cases.

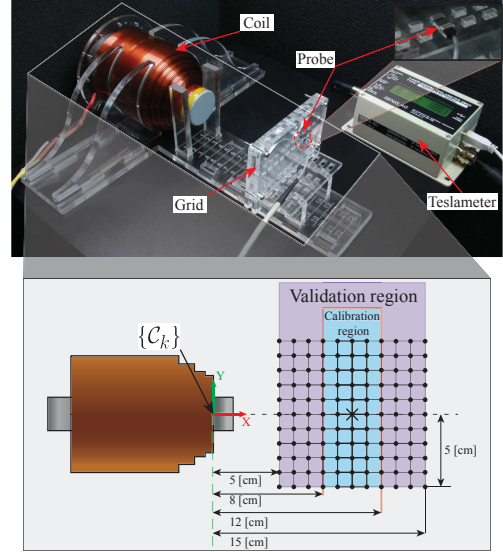


Fig. 4. The top image presents the workbench used for measurement of magnetic field. The detachable grid has 11 holes for Senis 3MH3A-500MT (Senis AG, Baar, Switzerland) Teslameter probe, at 1 cm from one another. As BigMag coils are axially symmetric, data comes from a single centre plane. The field is measured at a total of 121 locations, indicated by the corners of the grid on the bottom drawing. 400 data-points, spanning the full operational current range (-8 to 8 A), are collected for each location.

#### B. Validation of BigMag Model

This section aims at testing the performance of BigMag, along with its mathematical model, described by (6). The adjusted field models (with  $\epsilon = 6$ ) are used to build a currents-to-field map for the entire system through (4). This mapping is used to steer the magnetic field at the centrepoint of the workspace. The currents generated this way are prescribed for each coil. Thereafter, both of BigMag frames undergo arbitrary motions, while the magnetic field is measured for various points inside the workspace. This experiment is used to validate relation (6).

TABLE III  
THE ERRORS BETWEEN THE MAGNITUDE OF MAGNETIC FIELDS MEASURED AND ESTIMATED BY FINITE ELEMENT MODEL FOR UNCORRECTED DATA, AND CONSTANT COEFFICIENT ( $\gamma = 0$ ) AND EXPONENTIAL ( $\epsilon = 6$ ) CORRECTION.

Correction	Measure	Coils 1-4	Coils 5-6
Uncorrected	Mean [%]	15.74	11.06
	Standard Deviation [%]	9.08	4.01
Constant	Mean [%]	8.35	4.65
	Standard Deviation [%]	11.27	3.77
Exponential	Mean [%]	3.36	2.23
	Standard Deviation [%]	5.62	2.95

First investigation tests the capabilities of BigMag in steering of the magnetic field. All coils are kept coplanar with their configuration shown in Figure 2. This reduces the problem to two dimensions. Hence, the behaviour of the field can be modelled as follows:

$$\mathbf{B}_G(\mathbf{p}_G, \theta) = \|\mathbf{B}_G\| \begin{bmatrix} \sin(\theta) \\ 0 \\ \cos(\theta) \end{bmatrix} = [\beta_{C_1} \beta_{C_2} \dots \beta_{C_6}] \mathbf{I}, \quad (8)$$

$$\mathbf{I} = [I_1 \ I_2 \ \dots \ I_n]^T, \quad (9)$$

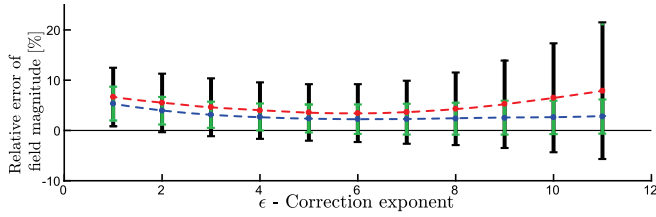


Fig. 5. The accuracy of correction proposed in (7) is measured for a range of candidate exponents ( $\epsilon$ ). The results show mean error (marks) and standard deviation (bars) for field estimates against the measured data at different exponents. The measurements were collected from validation regions (Figure 4) of stepped coil (red marks/black bars) and air-core coil (blue marks/green bars). For  $\epsilon = 6$  the average relative error is minimal for both datasets, hence this value was chosen for the rest of the investigation.

where  $\beta_{C_n} = \mathbf{R}_{C_n}^G \hat{\mathbf{B}}_{C_n}(\mathbf{p}_{C_k})$ . We use (7) to obtain  $\hat{\mathbf{B}}_{C_n}, \mathbf{I}$  for every  $n$ . Thereafter, we solve (8) for  $\|\mathbf{B}_G\|$  and  $\theta$  using Moore-Penrose pseudoinverse. This proposed model is tested as presented in Figure 6.

The experiment validates the model presented in Section III. The coils of BigMag are set to follow two different trajectories. The magnetic field for orientations ( $\mathbf{R}_{C_k}^G$ ) of the coils and the currents ( $\mathbf{I}$ ) along the trajectories are measured for nine points inside the workspace (see Figure 7). **Please also refer to the video accompanying this publication for demonstration of BigMag validation.**

For each data point from the experiment presented in Figure 7, the field estimate is calculated using (6) and (7). The mean relative error between the measurements and the estimates of the field is  $15.21 \pm 8.50\%$  for magnitude and for  $9.40 \pm 7.02^\circ$  for orientation. The principal cause of those discrepancies is the model overestimating the field at high magnitudes of  $B_x$  and  $B_y$ , most likely due to saturation of cores and cross-magnetization between neighbouring coils. The mean  $R^2$  correlation coefficients between measured and modelled magnetic fields are 0.967, 0.982 and 0.995 for  $B_x$ ,  $B_y$  and  $B_z$  respectively for data from all trajectories.

### C. Steering of Magnetic Catheters – Preliminary Test

The final experiment is performed to evaluate the possibility of steering magnetic catheters inside confined space using BigMag. A test bed is designed to mimic branching

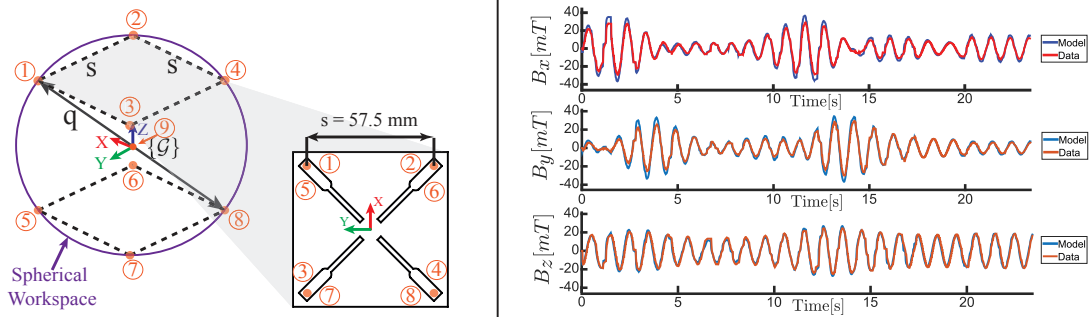


Fig. 7. To validate BigMag model, the field is measured at points 1-9 for two different motions. Points 1-8 are the corners of the biggest cube that can fit into BigMag workspace (with the edge  $s = 57.5$  mm). Point 9 is located at the centre of the workspace. The measurements are taken using 3MH3A-500MT teslameter (Senis AG, Baar, Switzerland), for two motions involving both frames rotating along the  $Z$  axis of frame  $\{G\}$ . The speeds are ( $\omega_t = \omega_b = -2$  RPM) for the first motion, and ( $\omega_t = 1.5$  RPM), ( $\omega_b = -3$  RPM) for the second one.  $\omega_t$  and  $\omega_b$  represent the angular velocities for top and bottom frames respectively. The currents of the coils followed the trajectories generated for the centrepoint of the workspace in the rotating field experiment (Figure 6), however for the second motion  $\|\mathbf{B}_G\| = 20$  mT. The plots on the right show the measured and modelled:  $B_x$ ,  $B_y$  and  $B_z$  components of the magnetic field, measured at location 4 for trajectory 2. The mean relative error for all trajectories is  $15.21 \pm 8.50\%$  for field magnitude and for  $9.40 \pm 7.02^\circ$  for orientation. **Please refer to the video accompanying this publication for demonstration of the measuring grid and the experiment.**

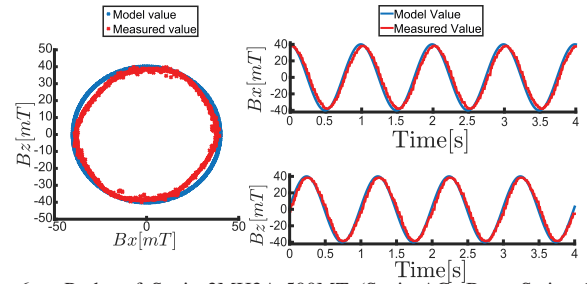


Fig. 6. Probe of Senis 3MH3A-500MT (Senis AG, Baar, Switzerland) is located in the centre of the workspace ( $\mathbf{p}_G = [0 \ 0 \ 0]^T$ ). For that point relation (8) is tested with BigMag for field oscillating with constant frequency ( $\dot{\theta} = 1$  Hz,  $\theta(0) = 0$ ) and  $\|\mathbf{B}_G\| = 40$  mT. Left: plot of  $B_x$  and  $B_z$  magnitudes of the magnetic fields measured during the field rotation. As the desired magnitude of the field is constant, the data-points should trace a circle. Right: plots of the same  $B_x$  and  $B_z$  components of the field against time.  $R^2$  coefficients are 0.964 and 0.973 for  $B_x$  and  $B_z$  respectively. The mean error of  $\|\mathbf{B}_G\|$  is 7.51%.

blood vessels. Several prototypes of magnetic catheters with different composition (see Table IV), are inserted into it using BigMag advancer. All prototypes bear a single, axially-magnetized, ring-shaped magnet mounted at their tip. Those catheters are examples of simple continuum manipulators. During the experiments the test bed is oriented vertically on the centre plane of the system. All six coils are aligned with that plane. Figure 8 presents the methods and results.

## V. CONCLUSIONS AND FUTURE WORK

In this paper we have presented BigMag, a novel platform using an array of mobile coils for 3D magnetic actuation of continuum manipulators. Furthermore, we have proposed and validated a mathematical model of its magnetic field. Finally, we have also demonstrated the application of BigMag for manual steering of magnetic catheters.

BigMag fulfils all of the requirements established during its design process. It provides functional workspace sufficient for trials on *ex vivo* specimen and on models of human heart. The system generates magnetic fields of at least 40 mT in any direction within its workspace, and provides gradients of up to 1 T/m. The models of the field show 3.36% maximum average error for field magnitude for a single coil, and

TABLE IV  
SPECIFICATION OF THE PROTOTYPES OF MAGNETIC CATHETERS.

Name	Material	Inner diameter	Outer diameter
T1	Pebax 6333	1.2 mm	2.2 mm
T2	Unidentified	1.1 mm	1.5 mm
T3	DEHP	1.2 mm	2.2 mm
T4	Shore 60A	1.0 mm	1.8 mm

15.21% for the entire system. The modelled and measured field trajectories correlate with a minimum  $R^2$  of 0.967.

The presented models are shown to overestimate the magnetic field at high currents. This may be an evidence of non-linear phenomena, such as saturation or cross-magnetization of the cores. In our future work, we plan to employ advanced models or on-line estimation of the fields to alleviate this problem. Moreover, in this paper we present only the experiments using manual steering. Hence, our next steps will involve demonstrating the full potential of the system. We plan to apply BigMag in automated, closed-loop steering of continuum manipulators, under the guidance of clinically-relevant tracking modalities.

#### REFERENCES

[1] P. Gomes, "Surgical robotics: Reviewing the past, analysing the present, imagining the future," *Robotics and Computer-Integrated Manufacturing*, vol. 27, no. 2, pp. 261–266, 2011.

[2] J. Burgner-Kahrs, D. C. Rucker, and H. Choset, "Continuum Robots for Medical Applications: A Survey," *IEEE Transactions on Robotics*, vol. 31, no. 6, pp. 1261–1280, 2015.

[3] R. J. Webster and B. A. Jones, "Design and Kinematic Modeling of Constant Curvature Continuum Robots: A Review," *The International Journal of Robotics Research*, vol. 29, no. 13, pp. 1661–1683, 2010.

[4] R. E. Goldman, A. Bajo, and N. Simaan, "Compliant motion control for multi-segment continuum robots with actuation force sensing," *IEEE Transactions on Robotics*, vol. 30, no. 4, pp. 890–902, 2014.

[5] A. Ali, D. H. Plettenburg, and P. Breedveld, "Steerable Catheters in Cardiology: Classifying Steerability and Assessing Future Challenges," *IEEE Transactions on Biomedical Engineering*, vol. 63, no. 4, pp. 679–693, 2016.

[6] I. A. Gravagne and I. D. Walker, "Manipulability, force, and compliance analysis for planar continuum manipulators," *IEEE Transactions on Robotics and Automation*, vol. 18, no. 3, pp. 263–273, 2002.

[7] G. J. Vrooijink, T. Ellenbroek, P. Breedveld, J. G. Grandjean, and S. Misra, "A preliminary study on using a Robotically-Actuated Delivery Sheath (RADS) for transapical aortic valve implantation," *2014 IEEE International Conference on Robotics and Automation (ICRA)*, Hong Kong, China, pp. 4380–4386, 2014.

[8] D. C. Rucker, B. A. Jones, and R. J. Webster, "A geometrically exact model for externally loaded concentric-tube continuum robots," *IEEE Transactions on Robotics*, vol. 26, no. 5, pp. 769–780, 2010.

[9] T. Kimura, S. Takatsuki, A. Oishi, M. Negishi, S. Kashimura, Y. Katsumata, T. Nishiyama, N. Nishiyama, Y. Tanimoto, and Y. Aizawa, "Operator-blinded contact force monitoring during pulmonary vein isolation using conventional and steerable sheaths," *International journal of cardiology*, vol. 177, no. 3, pp. 970–976, 2014.

[10] H. Tillander, "Magnetic guidance of a catheter with articulated steel tip," *Acta radiologica*, vol. 35, no. 1, pp. 62–64, 1951.

[11] A. Kangarlu, R. E. Burgess, H. Zhu, T. Nakayama, R. L. Hamlin, A. M. Abduljalil, and P. M. L. Robitaille, "Cognitive, cardiac, and physiological safety studies in ultra high field magnetic resonance imaging," *Magnetic resonance imaging*, vol. 17, no. 10, pp. 1407–1416, 1999.

[12] M. P. Kummer, J. J. Abbott, B. E. Kratochvil, R. Borer, A. Sengul, and B. J. Nelson, "Octomag: An electromagnetic system for 5-DOF wireless micromanipulation," *IEEE Transactions on Robotics*, vol. 26, no. 6, pp. 1006–1017, 2010.

[13] V. N. T. Le, N. H. Nguyen, K. Alameh, R. Weerasooriya, and P. Prattan, "Accurate modeling and positioning of a magnetically controlled catheter tip," *Medical Physics*, vol. 43, no. 2, pp. 650–663, 2016.

[14] J. Edelmann, A. J. Petruska, and B. J. Nelson, "Magnetic control of continuum devices," *The International Journal of Robotics Research*, vol. 36, no. 1, pp. 68–85, 2017.

[15] F. Carpi and C. Pappone, "Stereotaxis Niobe® magnetic navigation system for endocardial catheter ablation and gastrointestinal capsule endoscopy," *Expert review of medical devices*, vol. 6, no. 5, pp. 487–498, 2009.

[16] K. J. Boskma, S. Scheggi, and S. Misra, "Closed-loop control of a magnetically-actuated catheter using two-dimensional ultrasound images," *2016 6th IEEE RAS/EMBS International Conference on Biomedical Robotics and Biomechanics (BioRob)*, Singapore, pp. 61–66, 2016.

[17] B. Véron, A. Hubert, J. Abadie, and N. Andreff, "Geometric analysis of the singularities of a magnetic manipulation system with several mobile coils," *2013 IEEE/RSJ International Conference on Intelligent Robots and Systems*, pp. 4996–5001, 2013.

[18] F. Ullrich, S. Schuerle, R. Pieters, A. Dishy, S. Michels, and B. J. Nelson, "Automated Capsulorhexis Based on a Hybrid Magnetic-Mechanical Actuation System," *2014 IEEE International Conference on Robotics and Automation (ICRA)*, Hong Kong, China, pp. 4387–4392, 2014.

[19] F. P. Gosselin, V. Lalande, and S. Martel, "Characterization of the deflections of a catheter steered using a magnetic resonance imaging system," *Medical Physics*, vol. 38, no. 9, pp. 4994–5002, 2011.

[20] A. Gilroy, B. MacPherson, and L. Ross, *Atlas of Anatomy*, ser. Thieme Anatomy Series. Thieme, 2008.

[21] S. Miyashita, S. Guitron, M. Ludersdorfer, C. R. Sung, and D. Rus, "An untethered miniature origami robot that self-folds, walks, swims, and degrades," *2015 IEEE International Conference on Robotics and Automation (ICRA)*, Seattle, USA, pp. 1490–1496, 2015.

[22] C. Di Natali, M. Beccani, N. Simaan, and P. Valdastri, "Jacobian-Based Iterative Method for Magnetic Localization in Robotic Capsule Endoscopy," *IEEE Transactions on Robotics*, vol. 32, no. 2, pp. 327–338, 2016.

[23] D. J. Griffiths and C. Inglefield, *Introduction to Electrodynamics*, 3rd ed. Upper Saddle River, NJ: Prentice Hall, 2005.

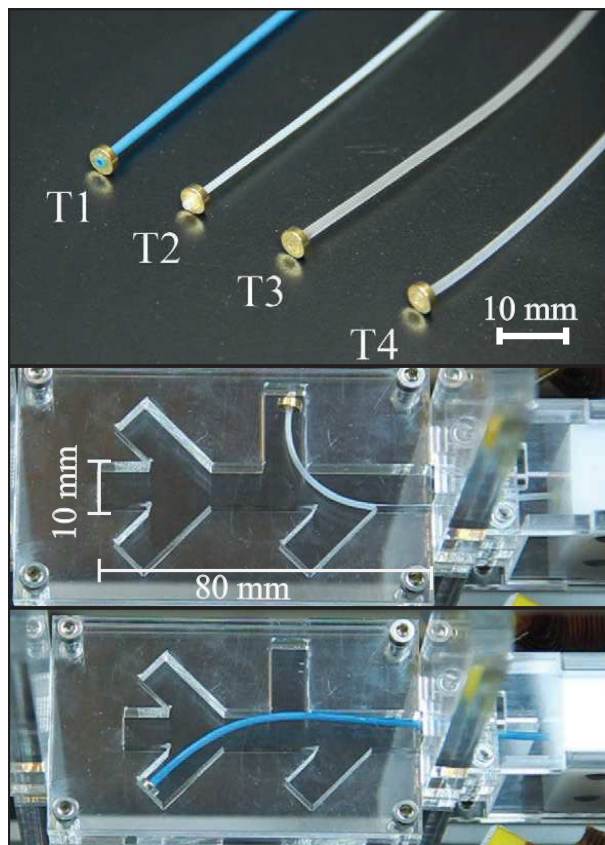


Fig. 8. Top: Magnetic catheters described in Table IV. Centre, bottom: The test bed is a 10 mm wide horizontal channel with four branches, angled at 45° and 90°. Currents in all coils and the position of the catheter inserter are all controlled by the operator using a keyboard to steer the catheters. All four devices are able to reach every prescribed destination during the experiments. **Please refer to the video accompanying this publication for demonstration of catheter steering.**